Journal of Materials Chemistry A

PAPER

View Article Online
View Journal | View Issue





Cite this: J. Mater. Chem. A, 2018, 6, 383

# Impact of rotamer diversity on the self-assembly of nearly isostructural molecular semiconductors†

Caitlin McDowell,[a] Kamatham Narayanaswamy,[b] Bommaramoni Yadagiri,[b] Thumuganti Gayathri,[b] Martin Seifrid,[a] Ram Datt,[c] Sean M. Ryno,[d] Michael C. Heifner,[d] Vinay Gupta,[c] Chad Risko,*[d] Surya Prakash Singh*[b] and Guillermo C. Bazan*[a]

Conformational diversity due to different orientations of structural subunits has a complex impact on morphological disorder of organic semiconductors. Here, we isolate the impact of a specific structural change: replacing bithiophene (biTh) units with thieno[3,2-*b*]thiophene (TT). We compare four molecules with an alternating donor–acceptor structure (D′–A–D–A–D′) composed of a central, electron-rich dithienosilole (DTS) unit flanked by pyridyl-[2,1,3]thiadiazole (PT) or fluorinated benzo[*c*][1,2,5]thiadiazole (FBT) and end-capped with bithiophene biTh or TT groups. We find that using TT instead of biTh results in an increased degree of order within films cast directly from solution by influencing the self-assembly tendencies of the different molecules. Unlike switching the acceptor subunit, such as FBT for PT, the TT for biTh structural change has little impact on the electronic structure of these molecular semiconductors. Instead, these morphological effects can be understood within the context of the predicted conformational diversity. TT units limit the number of rotational conformations (rotamers) available within this molecular architecture; low rotamer dispersity facilitates self-assembly into ordered domains. As a practical illustration of this greater drive toward self-assembly, we use the TT-containing molecules as donors in bulk heterojunction solar cells with $PC_{70}BM$. Devices with TT-containing molecules show improved photovoltaic performance compared to their previously characterized biTh analogs (d-DTS(PTTh$_2$)$_2$ and p-DTS(FBTTh$_2$)$_2$) in both as-cast and optimized conditions, with efficiencies up to 6.4% and 8.8% for **PT-TT** and **FBT-TT**, respectively. The TT subunit and, more broadly, the strategy of limiting conformational diversity can be readily applied toward the design of solution-processable organic semiconductors with increased as-cast order.

Received 12th November 2017
Accepted 22nd November 2017

DOI: 10.1039/c7ta09972j

rsc.li/materials-a

## Introduction

Organic semiconductors (OSCs) offer several potential advantages over their inorganic counterparts: low-cost production, mechanically flexible films, tunable optical and electronic response, and solution processability.[1–3] However, the optoelectronic performance of OSCs depends upon their ability to self-assemble into ordered phases in the solid-state during solvent deposition, a process that imposes considerable kinetic constraints.[4–6] Complex solvent mixtures and post-deposition treatment may be required to reach the solid-state morphology needed for optimal optoelectronic performance.[7,8] While the degree of order within OSC films can be estimated empirically by X-ray scattering techniques and relatively by changes in device performance,[4,9] there is still a vital need to understand what molecular substructures govern reliable self-assembly into ordered phases,[5] despite varying deposition conditions, which is key for all solution-processed OSC technologies. Indeed, substantial efforts have been dedicated toward distilling such structural design guidelines though the systematic study of OSC subunits, including backbone topology modification through conformational locking,[10] side-chain engineering to manipulate solubility,[11,12] blend miscibility,[13] and backbone planarity control.[14,15]

Conformational diversity due to different orientations of the component subunits has a complex impact on the possible solid-state structures and thus properties of organic crystals.[16,17] This is best illustrated by crystal engineering in the development of active pharmaceutical ingredients, as a drug's polymorphic form can strongly affect its bioavailability and dosing

[a]Department of Chemistry and Biochemistry, Center for Polymers and Organic Solids, University of California, Santa Barbara, USA. E-mail: bazan@chem.ucsb.edu
[b]Inorganic and Physical Chemistry Division, CSIR-Indian Institute of Chemical Technology, Uppal Road, Tarnaka, India. E-mail: spsingh@iict.res.in
[c]Organic and Hybrid Solar Cells, Physics of Energy Harvesting Division, CSIR-National Physical Laboratory, New Delhi-110012, India
[d]Department of Chemistry & Center for Applied Energy Research, University of Kentucky, Lexington, Kentucky 40506-0055, USA. E-mail: chad.risko@uky.edu

† Electronic supplementary information (ESI) available. See DOI: 10.1039/c7ta09972j

efficacy.[18–21] However, the effect of conformational polymorphism on morphological disorder in OSCs is comparatively less well understood.[22–25] In polymers, these contributions are difficult to distinguish from polydispersity effects, which may cause batch-to-batch variability in relevant properties. By contrast, molecular systems have both defined chemical structures and lengths, leading to less variable optical and electronic properties – in addition to offering ease of synthesis and purification.[1,3] The conformational space of molecular materials is also significantly smaller, making them better suited for understanding the complex and subtle influences of specific structural variations on material properties.[26]

In this work, we compare a set of four molecules with a modular architecture consisting of electron-donating (D) and accepting (A) subunits in a D′–A–D–A–D′ configuration. Our goal is to investigate the impact of a specific structural change: replacing bithiophene (biTh) units with thieno[3,2-*b*]thiophene (TT). All four molecules have the same central electron-donating dithienosilole (DTS) core, but use either pyridyl[2,1,3]thiadiazole (PT) or 6-fluoro-benzo[*c*][1,2,5]thiadiazole (FBT) as their electron-accepting subunits, and are capped with either electron-donating biTh or TT. For ease of comparison in this paper, we refer to these compounds as **PT-biTh**, **PT-TT**, **FBT-biTh** and **FBT-TT**, with structures shown in Fig. 1. **PT-TT** and **FBT-TT** were designed and synthesized for this study; **PT-biTh** was previously reported as d-DTS(PTTh$_2$)$_2$.[27–29] **FBT-biTh** (previously reported as p-DTS(FBTTh$_2$)$_2$) is a widely-studied molecular donor material in bulk heterojunction organic photovoltaics (BHJ OPVs).[30–33]

TT-containing polymeric semiconductors often show increased mobility in field-effect transistors (FETs)[34] and higher efficiency in OPVs[35,36] relative to their thiophene-derivatives. This improved performance has been attributed to greater order and closer π-stacking. However, there are counter examples: direct substitution of TT for thiophene or biTh yields little morphological or performance change in a PCDTBT analog,[37] and provides lower efficiency due to reduced morphological order in a polythiophene-based polymer.[38] We aim to better understand how the structural subunit TT influences self-assembly by comparing the molecular and bulk properties of **PT-TT** to **PT-biTh** and **FBT-TT** to **FBT-biTh** pairwise, using combined experimental and computational methods.

We find that substituting TT for biTh has minimal impact on the isolated molecular properties but influences the solid-state – as seen by optical absorbance, X-ray scattering and thermal analysis. Grazing-incidence wide-angle X-ray scattering (GIWAXS) reveals that the TT-containing molecules more readily form crystalline domains in both neat and blend films. For a demonstration of practical implementation, we used these molecules as donors in BHJ OPVs. The charge generation and transport mechanisms required for efficient photovoltaic performance rely on the self-assembly of specific structural features, including internal domains and interfaces between the donor and acceptor and continuous pathways for charge extraction.[4] This delicate BHJ morphology is often kinetically constrained by short solvent evaporation times and frustrated self-assembly of the blend components; however, it can be manipulated by solvent additives.[39] Despite negligible changes in molecular structure and electronic properties, **PT-TT** and **FBT-TT** outperform their biTh counterparts in OPV applications, particularly when cast directly from solution without additional processing. The changes in self-assembly and the resulting morphology when TT is substituted for biTh can be understood within the context of predicted conformational diversity.

## Results and discussion

### Synthesis and structure verification

Full details of the synthesis and characterization of **PT-TT** and **FBT-TT** can be found in the ESI.†

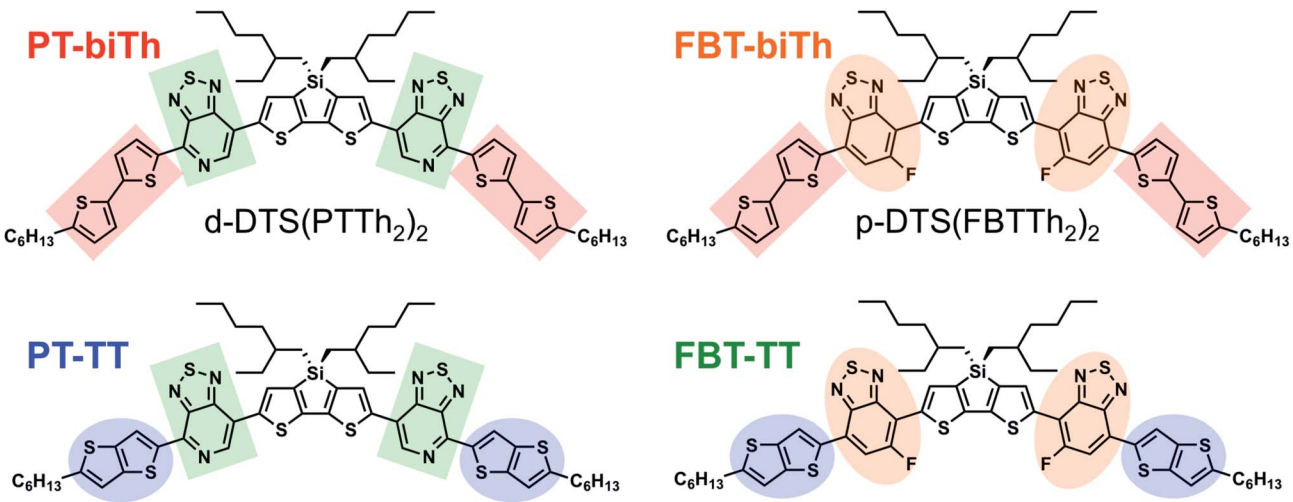


Fig. 1 Chemical structures of the four molecules in this study, emphasizing their constituent units: pyridylthiadiazole (PT, green), fluorobenzothiadiazole (FBT, orange), bithiophene (biTh, pink), and thieno[3,2-*b*]thiophene (TT, blue).

 

### Optical properties and electronic structure

The UV-visible absorption spectra of dilute solutions in chloroform are compared in Fig. 2a for **PT-biTh** and **PT-TT** and Fig. 2b for **FBT-biTh** and **FBT-TT**. The shape of the solution absorbance is nearly identical for all four molecules, with broad absorbance from 500 to 750 nm. The choice of electron-poor unit (PT or FBT) more strongly influences absorbance than that of the end-capping units; the peak absorbances of **FBT-biTh** and **FBT-TT** are blue-shifted by 0.13 eV from **PT-biTh** and **PT-TT**, respectively. TT substitution causes a slight blue shift of 0.05 eV in the absorbance of both **PT-TT** and **FBT-TT** but does not have a clear impact on molar absorptivity. Absorptivity is increased slightly for **PT-TT** (25% greater than **PT-biTh**) but decreased for **FBT-TT** (50% less than **FBT-biTh**).

In thin films cast from 20 mg $mL^{-1}$ chlorobenzene, the absorbance spectra of the four molecules broaden and red-shift out to 800 nm, as shown in Fig. 2c and d. All exhibit two principal absorption peaks. One of these peaks is a vibronic shoulder that appears at 700 nm for **PT-biTh** and **PT-TT**, and 690 nm for **FBT-biTh** and **FBT-TT**; the emergence of such fine structure indicates effective stacking of the π-conjugated backbones in as-cast neat films of all four molecules.[40–42] The optical band gaps (based on the onset of absorption) of the PT-derivatives in solution are approximately 0.15 eV less than their FBT-analogs, but this reduces to 0.04 eV in the solid state. We used cyclic voltammetry (CV) to determine the energy levels of the newly synthesized **PT-TT** and **FBT-TT** relative to ferrocene, as shown in Fig. S1.†

The optical properties and energy levels of all four molecules are presented in Table 1. Examining the PT- and FBT-containing molecules pairwise, TT and biTh appear to contribute equally to the electronic structure. Specifically, there are negligible differences in the redox potentials and absorbance features of **PT-TT** and **FBT-TT**, when compared to **PT-biTh** and **FBT-biTh**, respectively.

### Solid-state morphology and single crystal structure

GIWAXS was used to probe the thin film solid-state morphology of all four molecules. This diffraction technique has been used to correlate organizational tendencies of OSCs on the nanoscale to the observed properties of bulk thin films.[9,43] Solutions of each molecule were spun cast onto untreated silicon substrates under identical preparation and casting conditions to compare their internal thin-film order and propensity for self-assembly from solution.

GIWAXS shows that the diffraction patterns from as-cast films of **PT-TT** and **FBT-TT** exhibit altered packing structure and increased definition and texture compared to their biTh analogs. Changing from PT to FBT also increases the relative degree of thin-film order observed for these molecules, similar to other examples in the literature;[44,45] however, this is due to a convolution of changes in electronic structure as well as intra- and intermolecular interactions. To isolate the impact of the TT for biTh substitution, we focus on the molecules pairwise, with **PT-biTh** and **PT-TT** shown in Fig. 3, and **FBT-biTh** and **FBT-TT** shown in Fig. 4. A summary of crystalline features is provided in Table S1.†

From Fig. 3a, **PT-biTh** exhibits isotropic alkyl features at 0.32 $Å^{-1}$ and π-stacking features at 1.77 $Å^{-1}$. **PT-TT**, in Fig. 3b, has tighter alkyl packing at 0.38 $Å^{-1}$ with a similar π-stacking peak at 1.76 $Å^{-1}$. Notably, **PT-TT** orients preferentially edge-on relative to the substrate and, instead of **PT-biTh**'s broad

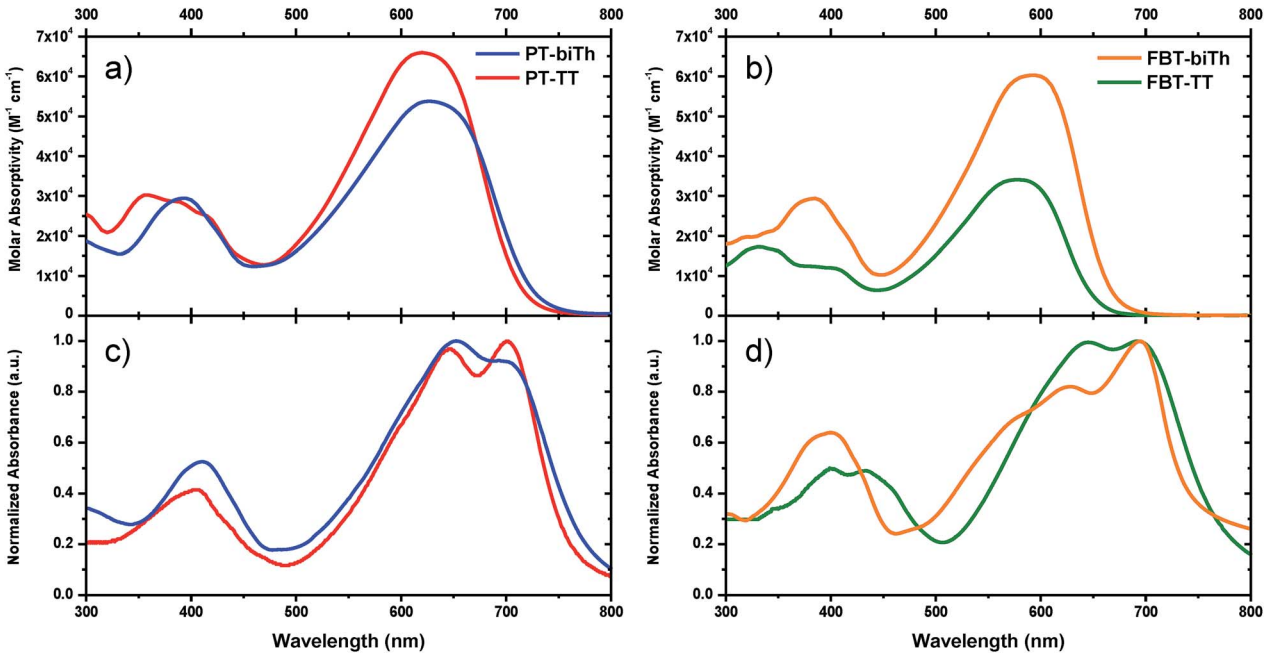


Fig. 2 Molar absorptivities ($M^{-1}$ $cm^2$) in dilute chlorobenzene solution of (a) PT-biTh and PT-TT, and (c) FBT-biTh and FBT-TT. Normalized film absorbance of (b) PT-biTh and PT-TT, and (d) FBT-biTh and FBT-TT.

Table 1 Optical properties and energy levels of the four molecules, summarizing the spectra in Fig. 2 and cyclic voltammetry in Fig. S1

| | Solution | | | | Thin film | | | Energy levels | | |
|---|---|---|---|---|---|---|---|---|---|---|
| Donor | $\lambda_{max}$ (nm) | $\lambda_{onset}$ (nm) | $E_{gap}$ (eV) | $\varepsilon$ ($M^{-1}$ $cm^{-1}$) | $\lambda_{max}$ (nm) | $\lambda_{onset}$ (nm) | $E_{gap}$ (eV) | HOMO (CV, eV) | LUMO (CV, eV) | $E_{gap}$ (eV) |
| **PT-biTh** | 630 | 730 | 1.70 | $5.43 \times 10^4$ | 710 | 780 | 1.59 | −5.26 (ref. 21) | −3.54 (ref. 21) | 1.72 |
| **PT-TT** | 615 | 710 | 1.74 | $6.76 \times 10^4$ | 700 | 770 | 1.61 | −5.24 | −3.56 | 1.68 |
| **FBT-biTh** | 590 | 665 | 1.87 | $6.07 \times 10^4$ | 690 | 760 | 1.63 | −5.12 (ref. 45) | −3.34 (ref. 45) | 1.78 |
| **FBT-TT** | 575 | 655 | 1.89 | $3.34 \times 10^4$ | 690 | 765 | 1.62 | −5.30 | −3.42 | 1.88 |

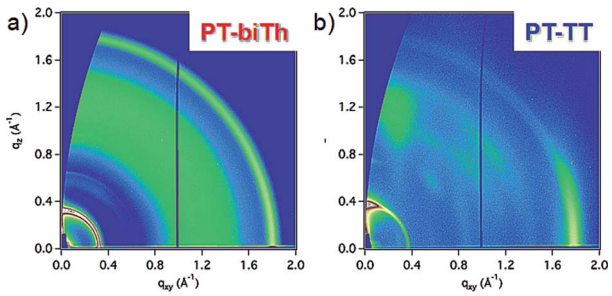


Fig. 3 GIWAXS images of (a) PT-biTh and (b) PT-TT.

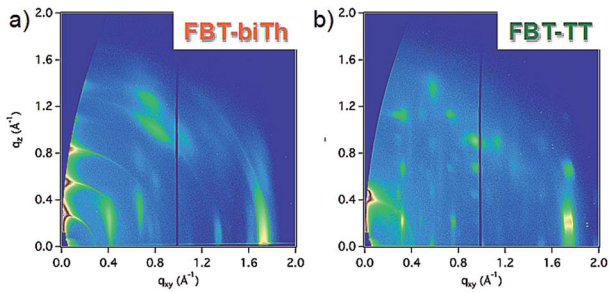


Fig. 4 GIWAXS images of (a) FBT-biTh and (b) FBT-TT.

isotropic band from 0.9–1.5 Å$^{-1}$, Bragg rods and diffraction spots are observed. Both of these features indicate increased order in as-cast **PT-TT**.

**FBT-biTh** and **FBT-TT** display distinct diffraction spots in Fig. 4 and have strong Bragg reflections parallel to the $q_z$ axis. While the alkyl-stacking feature at 0.41 Å$^{-1}$ of **FBT-TT** does not exhibit overtones like **FBT-biTh** in Fig. 4a, more distinct spots are seen off-axis, even at high $q$-values. This quality is most strongly seen for the π-stacking peak at 1.75 Å$^{-1}$, which is 5° off the $q_{xy}$ axis – indicating both long-range order and strong edge-on preferential orientation toward the substrate surface.[46] Interestingly, the alkyl stacking distances for both **PT-TT** and **FBT-TT** are significantly shorter than their biTh-analogs, while their π-stacking distances are comparable.

Single-crystal structures of molecular semiconductors, when available, can offer fundamental insight into their organizational tendencies.[29] The single-crystal structure of **FBT-biTh** has been characterized, allowing for in-depth analysis of its distinctive GIWAXS diffraction pattern.[29,30] In the **FBT-biTh** unit cell, π-stacking occurs between molecules with the same conformation and orientation, in a slip-stacked fashion.[24] The short-axis dipole moments of each molecule within the stack are oriented together, canceled by an adjacent anti-symmetric stack. The repeat ordering of the two molecular stacks results in the large 2.33 nm alkyl spacing seen in **FBT-biTh** thin films.[24]

Slow diffusion of acetonitrile into a dilute chloroform solution of **FBT-TT** yielded single crystals suitable for structure determination. Features of the crystal structure are shown in Fig. 5. **FBT-TT** exhibits a different packing motif than **FBT-biTh** and is consistent with the observed features in its the GIWAXS pattern. Unlike **FBT-biTh**, molecules of **FBT-TT** are interleaved with close π-stacking occurring between pairs of anti-symmetric molecules in a single stack (Fig. 5c). The repeat spacing occurs across one molecular backbone, rather than two, resulting in the shorter alkyl spacing of 1.77 nm (Fig. 5b). This packing structure is also denser (at 1.332 g cm$^{-3}$) than **FBT-biTh** (at 1.267 g cm$^{-3}$), despite the lower molecular mass of **FBT-TT**. There are partial probabilities of multiple conformations of **FBT-TT** present in the crystal structure, *i.e.* disorder, which will be discussed further in Section 2.7.

### Thermal transitions by DSC

The thermal transitions of the four molecules were investigated using differential scanning calorimetry (DSC) measurements under a nitrogen atmosphere – please refer to Fig. S2.† All four exhibit reversible melting and crystallization behavior, indicating the presence of crystalline phases. **PT-TT** has an increased melting temperature ($T_m$ = 254 °C) and enthalpy of melting ($\Delta H_m$ = 51.7 J g$^{-1}$) relative to **PT-biTh**'s major melting transition at 220 °C ($\Delta H_m$ = 35.5 J g$^{-1}$). **PT-biTh** exhibits a minor exothermic transition at a lower temperature ($T_m$ = 120 °C), indicative of polycrystallinity or a possible liquid crystalline state; **FBT-biTh** also exhibits a weak exotherm at 150 °C, visible only with rapid heating rates above 100 °C min$^{-1}$, which is attributed to a liquid crystalline transition.[47] However, **PT-TT** exhibits only one exothermic transition. These differences imply that **PT-TT** likely exhibits stronger intermolecular interactions in the solid state that favor one crystalline form.

Substituting TT for biTh into the **FBT-biTh** molecular framework lowers the thermal transitions, as seen in Fig. S2b.† One observes that the melting point decreases from 211 °C for **FBT-biTh** to 178 °C for **FBT-TT**, and the crystallization temperature decreases from 185 °C to 152 °C. Notably, the enthalpy of melting ($\Delta H_m$) of **FBT-TT** is significantly lower, 15.7 J g$^{-1}$ *vs.* 61.0 J g$^{-1}$. This exotherm was confirmed as melting transition

 

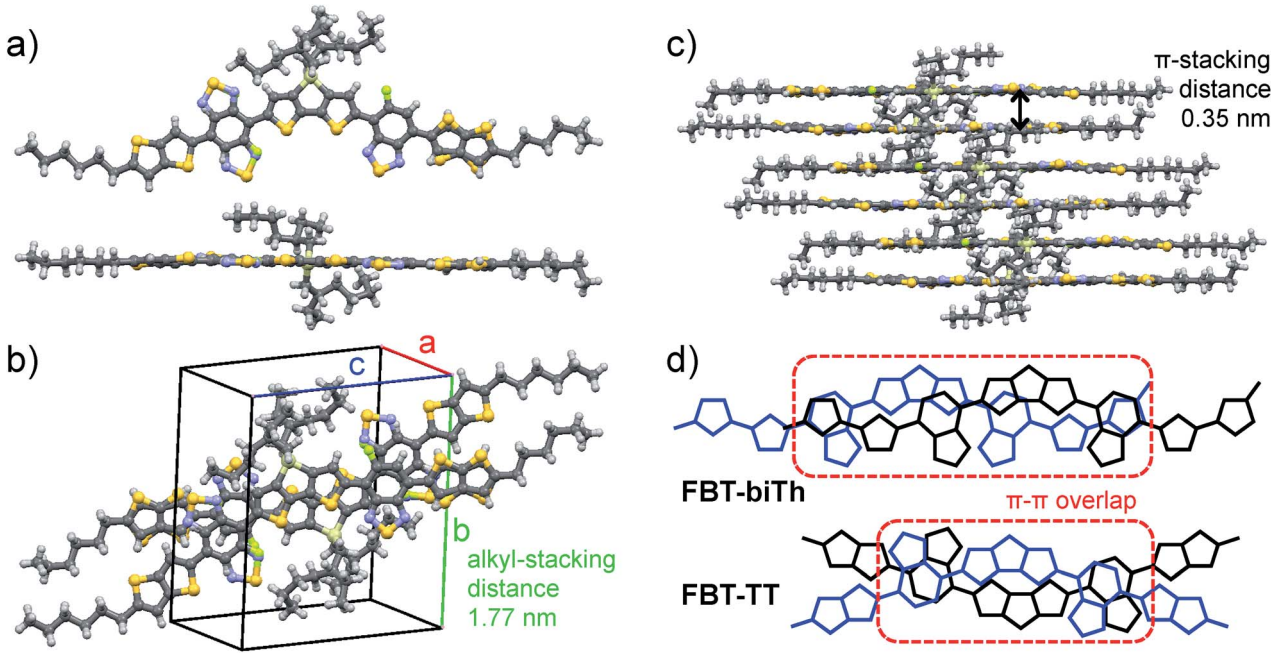


Fig. 5 Structural details obtained through single X-ray diffraction of FBT-TT. (a) Molecular conformation of FBT-TT with C, N, S and F atoms shown in grey, blue, yellow, and green respectively. (b) Unit cell showing 1.77 nm alkyl spacing, oriented approximately along the b-vector. (c) Packing viewed along the (102) plane to highlight π-stacking and hexyl-stacking. (d) Skeletal schematic showing the overlap of π-conjugated backbone between adjacent molecules in FBT-biTh and FBT-TT crystals.

by loss of X-ray diffraction peaks from thin films during heating, shown in Fig. S3.† The lower enthalpies of **FBT-TT**'s transitions, compared to **FBT-biTh**, likely arise from a reduction in the degree of π–π overlap between adjacent molecular backbones in its crystal structure, as shown in Fig. 5d. Thus, fusing biTh into TT substantially influences the stability of the crystalline phase by changing the dominant packing structure favored by **FBT-TT**, despite similar molecular connectivity.

### Photovoltaic performance

Crystalline domains with long-range order are usually sought after with efficient charge transport in organic semiconductor applications, such as in transistors and solar cells.[48] Photovoltaic performance provides insight into how a material's self-assembly tendencies translate into bulk properties under various kinetic constraints, such as the blend ratio, choice of solvent(s) and other deposition parameters. Materials that are less sensitive to processing also tend to exhibit strong self-assembly tendencies.[47,49,50] Thus, by comparing the blend film morphology and photovoltaic performance of these four molecules, we can probe how their self-assembly tendencies withstand kinetically constrained film forming conditions and isolate the role of TT in directing self-assembly.

We used the OPV device fabrication conditions and optimization protocols published for **PT-biTh**:$PC_{70}BM$[27,28] and **FBT-biTh**:$PC_{70}BM$,[30,51] respectively, allowing for direct comparison to literature performance values. Details of the device fabrication, optimization and processing conditions are presented in the ESI.† 1,8-Diiodooctane (DIO) was used as processing additive alter the morphology and resulting performance of the active layer.[52] Photovoltaic performance has been shown to improve due to the higher degree phase separation and increased donor domain purity in blend films processed by DIO.[53–55] Notably, the best device performances for **PT-TT**:$PC_{70}BM$ and **FBT-TT**:$PC_{70}BM$ were achieved for the same donor : acceptor blend ratios and DIO concentrations as **PT-biTh**:$PC_{70}BM$ and **FBT-biTh**:$PC_{70}BM$, respectively. These similarities simplify comparison of their resulting film morphologies and performance. As-cast and optimized device characteristics are summarized in Table 2. Representative current–voltage curves under AM 1.5 G illuminations (100 mW $cm^{-2}$) are shown in Fig. 6. Traces for **PT-biTh**:$PC_{70}BM$[28] and **FBT-biTh**:$PC_{70}BM$[51] from the literature are also provided in grey.

BHJ solar cells were fabricated with a ITO/MoOx/**PT-TT**:$PC_{70}BM$/Al architecture, to prevent detrimental interactions with the widely-used PEDOT:PSS hole-transport layer.[28] Open-circuit voltage ($V_{oc}$) values are similar for the two PT-derivatives, which is expected given their similar HOMO levels. However, **PT-TT**:$PC_{70}BM$ significantly improves upon the as-cast PCE of **PT-biTh**:$PC_{70}BM$ (from 2.5 to 4.2%), largely due to increases in short-circuit current ($J_{sc}$) and fill factor (FF). We attribute this to a greater degree of donor organization in **PT-TT**:$PC_{70}BM$ as-cast, as observed by GIWAXS in Fig. 7c. The highest efficiencies were obtained from devices cast from solutions containing 0.25% DIO by volume, the same required for **PT-biTh**.[28] Not surprisingly, **PT-TT**:$PC_{70}BM$ also outperforms **PT-biTh**:$PC_{70}BM$ processed with DIO, with average PCEs of 6.4% (see Fig. S5a†), compared to **PT-biTh**'s 5.6%.

FBT-containing molecules are less sensitive to the acidity of the PEDOT:PSS layer than PT-containing molecules,[51] so the

Table 2 Average current–voltage characteristics of solar cells whose active layers contain the four molecules blended with $PC_{70}BM$ and optimized DIO concentration (v/v)

| | Active layer | D : A ratio | DIO (v/v%) | $V_{oc}$ (V) | $J_{sc}$ (mA cm$^{-2}$) | FF (%) | PCE (%) | Number of devices |
|---|---|---|---|---|---|---|---|---|
| As-cast | **PT-biTh**:$PC_{70}BM$[22] | 7 : 3 | 0 | 0.75 | 8.9 | 37 | 2.5 | — |
| | **PT-TT**:$PC_{70}BM$ | 7 : 3 | 0 | 0.74 ± 0.02 | 11.4 ± 0.2 | 47 ± 1 | 4.2 ± 0.2 | 20 |
| | **FBT-biTh**:$PC_{70}BM$[45] | 6 : 4 | 0 | 0.78 | 6.6 | 36 | 1.8 | — |
| | **FBT-TT**:$PC_{70}BM$ | 6 : 4 | 0 | 0.85 ± 0.02 | 11.4 ± 0.2 | 55 ± 1 | 5.4 ± 0.3 | 15 |
| With DIO[a] | **PT-biTh**:$PC_{70}BM$[22] | 7 : 3 | 0.25 | 0.73 | 12.7 | 60 | 5.6 | — |
| | **PT-TT**:$PC_{70}BM$ | 7 : 3 | 0.25 | 0.74 ± 0.01 | 13.4 ± 0.1 | 64 ± 1 | 6.4 ± 0.1 | 40 |
| | **FBT-biTh**:$PC_{70}BM$[45] | 6 : 4 | 0.4 | 0.81 | 12.8 | 68 | 7.0 | — |
| | **FBT-TT**:$PC_{70}BM$ | 6 : 4 | 0.4 | 0.84 ± 0.01 | 14.3 ± 0.1 | 73 ± 1 | 8.8 ± 0.2 | 45 |

[a] Devices processed with DIO were annealed at 80 °C for 15 minutes after spin-casting, to drive off residual solvent.

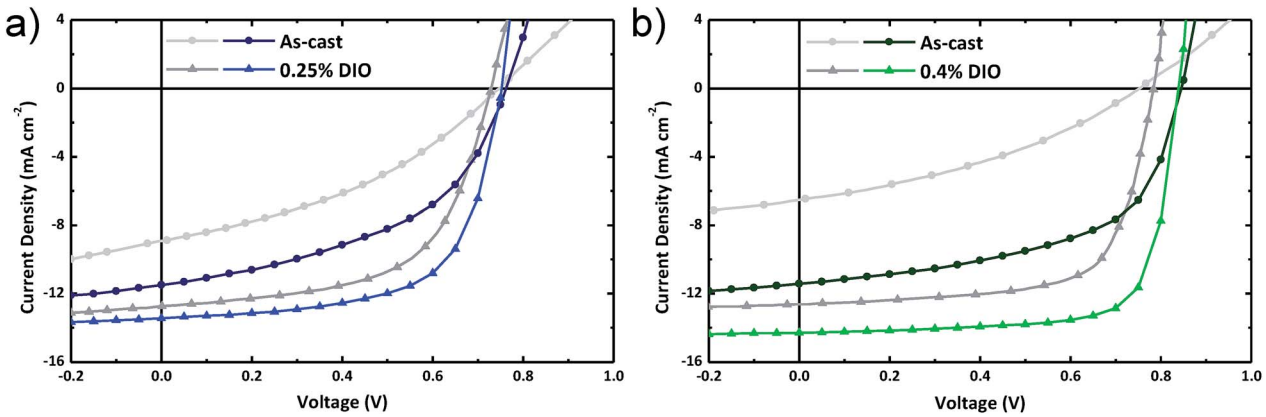


Fig. 6 Representative current–voltage curves (a) **PT-TT**:$PC_{70}BM$ (blue, compared to **PT-biTh**:$PC_{70}BM$[22] in grey), and (b) **FBT-TT**:$PC_{70}BM$ (green, compared to **FBT-biTh**:$PC_{70}BM$[45] in grey). Both as-cast (circles) and optimized DIO additive (triangles) devices are represented.

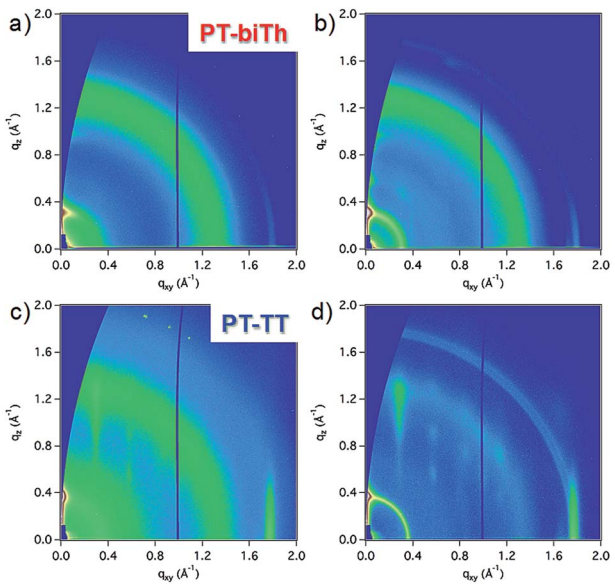


Fig. 7 2D GIWAXS images of bulk heterojunction films of (a) as-cast **PT-biTh**:$PC_{70}BM$, (b) **PT-biTh**:$PC_{70}BM$ with 0.25% v/v DIO, (c) as-cast **PT-TT**:$PC_{70}BM$, and (d) **PT-TT**:$PC_{70}BM$ with 0.25% v/v DIO.

ITO/PEDOT:PSS/**PT-TT**:$PC_{70}BM$/Al architecture was used. **FBT-biTh**:$PC_{70}BM$ exhibits a low performance as-cast (PCE of 1.8%), but improves to 7.0% upon processing with DIO. As-cast blends of **FBT-TT**:$PC_{70}BM$ exhibit a PCE of 5.4%, a significant improvement over the as-cast performance of **FBT-biTh**:$PC_{70}BM$. Improved FF and $J_{sc}$ suggest more facile self-assembly into the desirable morphology during the evaporation of the chlorobenzene solvent. Like with **FBT-biTh**:$PC_{70}BM$, **FBT-TT**:$PC_{70}BM$ exhibits signs of more efficient charge extraction when processed with 0.4% DIO additive,[56–58] such as a high fill factor of 73% and an external quantum efficiency (EQE) of 74%. Optimized **FBT-TT**:$PC_{70}BM$ blend films achieve PCEs of 8.8 ± 0.1% over an average of 45 devices (see Fig. S5b†). The recorded maximum of 9.1% for **FBT-TT**:$PC_{70}BM$ is comparable with the highest performances observed for small molecule donors with $PC_{70}BM$.[59–61]

## Blend film morphology by GIWAXS

We used GIWAXS to examine morphological differences between as-cast molecule:$PC_{70}BM$ films under the same deposition conditions as for the devices in Table 2. GIWAXS images of the PT-derivatives are shown in Fig. 7, and the

 

FBT-derivatives in Fig. 8. Table S1 in the ESI† lists a summary of the GIWAXS data for ease of comparison.

The alkyl-stacking and π-stacking features in **PT-biTh**:$PC_{70}BM$ blends in Fig. 7a show more edge-on character than in neat donor films. None of **PT-biTh**'s other diffraction features for can be distinguished against $PC_{70}BM$'s isotropic band at ~1.35 $Å^{-1}$.[62] **PT-biTh**:$PC_{70}BM$ film processed with DIO have longer range order and surface texture than in neat films, evidenced by additional overtones of the alkyl stacking peak and the appearance of off-axis features in Fig. 7b. In Fig. 7c, **PT-TT** retains its well-defined diffraction features in $PC_{70}BM$ blend films, such as the Bragg rods at 0.3 and 0.6 $Å^{-1}$ along the $q_{xy}$ axis. The definition of these features increases with DIO processing (shown in Fig. 7d), resulting in longer crystalline correlation lengths (CCLs, see ESI†).

Both **FBT-biTh**:$PC_{70}BM$ and **FBT-TT**:$PC_{70}BM$ exhibit low donor crystallinity as-cast. This low degree of order is expected for **FBT-biTh**, which previous GIWAXS studies have shown is kinetically trapped in a metastable liquid crystalline state, with a distinct alkyl feature at 0.45 $Å^{-1}$.[31] The features seen in Fig. 8a are consistent with a **FBT-biTh**:$PC_{70}BM$ film that is transitioning between the metastable phase to the desired crystal form seen in neat films. DIO allows for a more rapid conversion between the metastable and crystalline phases, with most of the development occurring an hour after deposition.[41] Accordingly, **FBT-biTh**:$PC_{70}BM$ films processed with 0.4% DIO exhibit strong donor diffraction features (see Fig. 8b).

The frustrated self-assembly of **FBT-TT** evidenced in Fig. 8c is unexpected; the most prominent feature of as-cast **FBT-TT**:$PC_{70}BM$ films is the isotropic fullerene band at ~1.35 $Å^{-1}$.[63] No evidence of a metastable phase was observed by DSC or when comparing the as-cast and DIO-processed GIWAXS. However, the features of crystalline **FBT-TT** in Fig. 8d bear a striking resemblance to those expected for the **FBT-biTh** metastable phase: the alkyl-stacking peak at 0.41 $Å^{-1}$ by GIWAXS in Fig. 4b, and lower melting temperature and enthalpy by DSC in Fig. S2.† This suggests that the metastable phase of **FBT-biTh** could have similar features to the **FBT-TT** crystal structure, such as interleaved anti-symmetric pairs that reduce the degree of π–π overlap when compared to the slip-stacked symmetric pairs in the **FBT-biTh** crystal structure (Fig. 5d).

The GIWAXS results described above indicate that the TT moiety promotes molecular self-assembly into ordered phases more so than biTh. Formation of large donor domains directly from solution for **PT-biTh**:$PC_{70}BM$ is frustrated by the presence of the acceptor, resulting poor as-cast PCE. **PT-TT** (Fig. 7c) is less frustrated by $PC_{70}BM$, based on the presence of Bragg rods, resulting in more efficient photovoltaic output (Fig. 7a). However, the as-cast performance from **FBT-TT**:$PC_{70}BM$ of 5.4% is difficult to understand within the context of donor organization described by GIWAXS, compared to **FBT-biTh**:$PC_{70}BM$'s 1.8%, given that both blend films exhibit weak diffraction from the donor. **FBT-TT**:$PC_{70}BM$ films with 0.4% DIO (Fig. 8d) regain the distinct anisotropic scattering peaks corresponding to the donor, with greater spot resolution than in neat **FBT-TT** or **FBT-biTh**. It is possible that small crystallites are nucleated during the chlorobenzene drying period, which ripen considerably in the presence of the DIO solvent additive.[63] Thus, **FBT-TT** blend films processed with DIO achieve longer CCLs (see ESI†), which may be responsible for the improved PCEs over **FBT-biTh**:$PC_{70}BM$.

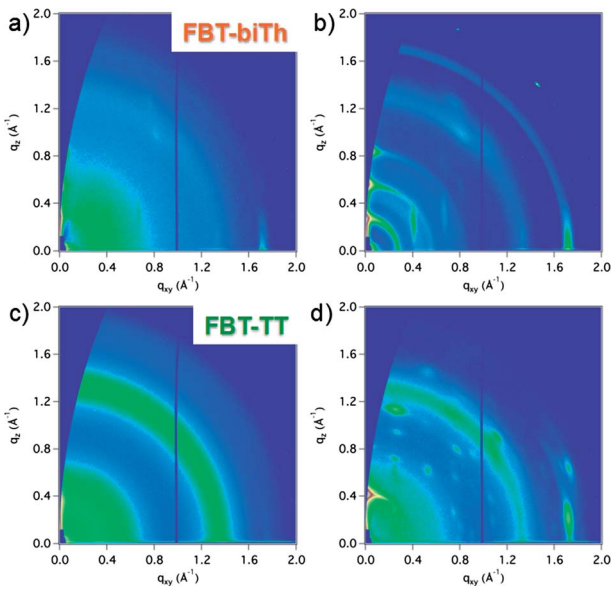


Fig. 8 2D GIWAXS images of bulk heterojunction films of (a) as-cast **FBT-biTh**:$PC_{70}BM$, (b) **FBT-biTh**:$PC_{70}BM$ with 0.25% v/v DIO, (c) as-cast **FBT-TT**:$PC_{70}BM$, and (d) **FBT-TT**:$PC_{70}BM$ with 0.25% v/v DIO.

## Rotational barriers and rotamer diversity

Structural variations in π-conjugated systems, like substituting TT and biTh, are expected to influence both conformational diversity and rates of self-assembly through non-covalent intramolecular (along the backbone) and intermolecular interactions. For example, the sulfur lone-pair electrons in thiophene can induce through-space interactions with adjacent atoms, such as F and H, that increase the rotational barrier between thiophene and subunits with these atoms.[64] Such conformational locks can enforce long-range planarity in π-conjugated molecules and polymers.[10,14,65] Likewise, dipole–dipole or hydrogen bonding interactions can be strong drivers of molecular packing.[15] To better understand why the TT for biTh substitution changes the observed self-assembly tendencies, we used computational methods to compare the respective influences of the biTh and TT units on rotational barriers, the number and distribution of possible molecular conformations, and the properties of the conformations most likely to be populated.

TT is expected to have similar conformational locking preferences with PT (or FBT) as biTh because it has S and C–H sites in the same geometric arrangement. The dihedral potential energy surfaces (PESs) between FBT and the adjacent fragments (biTh or TT) are shown in Fig. S8.† The PESs were calculated using density functional theory (DFT) at the ωB97X-D/6-31G(d,p) level of theory. As expected, the rotational barriers

are comparable in magnitude and shape, with minima at ~20° and 150°. The energy barrier for rotation between adjacent thiophenes (Th–Th) is estimated at 2.7 to 3.7 kcal $mol^{-1}$.[66,67] Thus, the observed differences in ability of **FBT-biTh** and **FBT-TT** to organize cannot be the result of increased conformational locking, as the rotational barriers between the FBT–biTh, FBT–biTh and Th–Th fragments are essentially identical.

We now consider the possible structural conformations available to the four molecules. The orientation of each backbone subunit can be arbitrarily designated up (U) or down (D) relative to the central dithienosilole unit. TT lacks the internal point of rotation of biTh, which reduces the number of inter-ring rotations along the D′–A–D–A–D′ backbone from six to four, as shown in Fig. 9. This structural exchange narrows the range of possible near planar rotational isomers (rotamers) from sixty-four ($2^6$) for biTh derivatives to sixteen ($2^4$) for the TT-analogs, see Table S5.† Asymmetric rotamers are degenerate – *i.e.* they are energetically equivalent to their mirror image – which reduces the number of unique conformations; the ten unique rotamers of **PT-TT** are shown in Fig. S9.† As illustrated in Fig. S10,† rotation within bithiophene leads **PT-biTh** and **FBT-biTh** to have four rotamers for each available to their TT-analogs.

Not all rotamers are equi-energetic. Intuitively, lower energy conformations are expected to have higher relative populations at a given temperature and may be anticipated to play a more influential role in determining the kinetics of crystallization. The growth of ordered domains may be slowed by the presence of rotamers with significantly different conformations or dipole moment vectors, due to changes in the nature and strength of their intermolecular non-covalent interactions. Dispersity, regardless of its provenance, has been shown to frustrate self-assembly and prevent long-range order in bulk films.[37,60] For example, replacing benzothiadiazole as the A moiety in this D′–A–D–A–D′ architecture with PT increases donor crystallinity and OPV performance.[28] The rotational barrier around the PT and biTh linkage is significantly higher than benzothiadiazole and biTh, which decreases the rotamer diversity and orients the rotamers' dipole moments along similar vectors. These factors are suggested to promote self-assembly and drive phase separation in PT-containing donors.[28] Substituting TT for biTh has similar potential to influence the distribution of thermally accessible rotamers.

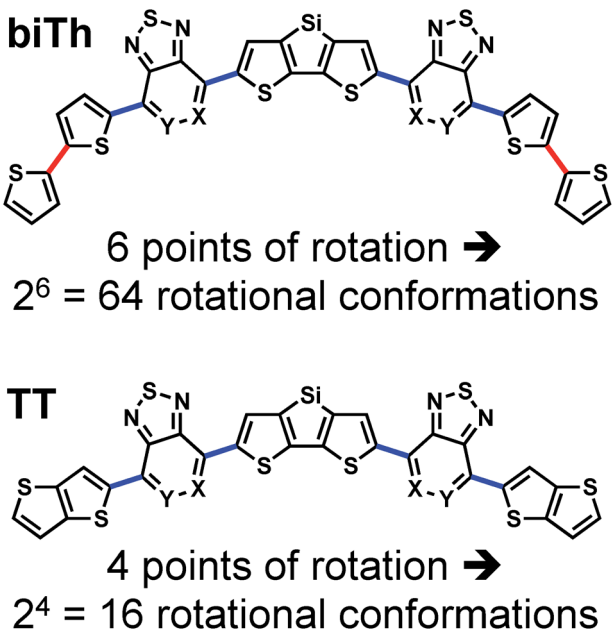


Fig. 9 Schematic of the two backbone D′–A–D–A–D′ structures, containing biTh or TT end-capping units. The number of points of rotation determines the possible number of rotamers, with common points of rotation highlighted in blue. PT-containing molecules have X = C–H, Y = N, and FBT-containing molecules have X = C–F, Y = C–H. Alkyl groups are omitted for clarity.

To investigate this, we determined the optimized geometry of each rotamer in Table S5† for all four molecules, at the ωB97X-D/6-31G(d,p) level of theory. From this, we obtained the relative energy and short-axis dipole moment of each rotamer. Transition state theory predicts that these molecules are thermally equilibrated within milliseconds at room temperature, as the energetic cost to rotation between each dihedral in Fig. 9 is small.[69] Thus, relative energy differences can be used to predict the thermally-accessible rotamers at 300 K using the Boltzmann distribution, irrespective of their starting conformations.[69] From the summary of these calculated quantities in Fig. 10, one observes that the overall energetic landscapes do not significantly change going from biTh- to TT-containing molecules, *e.g.* the change in energy across all rotamers of **PT-biTh** resembles that of **PT-TT** (5.3–5.6 kcal $mol^{-1}$) and the same is true for **FBT-biTh** and **FBT-TT** (3.0–3.5 kcal $mol^{-1}$). **PT-biTh** and **FBT-biTh** have more thermally-accessible species principally because their structures contain additional degrees of freedom with small energetic differences within that energy landscape.

The distribution of **PT-biTh** conformers is dominated by five states with relative populations greater than 0.2, while **PT-TT** has only two such states available. Both molecules have large short-axis dipole moments (on the order of 2 debye) that vary substantially with changing rotational conformation. These results suggest that not only could the self-assembly of **PT-biTh** be frustrated by the existence of multiple rotamer populations but also that dipolar disorder could impede the efficient formation of crystalline domains. **PT-TT**, on the other hand, is less affected by variation in rotamer population, but mismatched dipole orientation could still be problematic. This analysis is consistent with the relative degree of order shown by the GIWAXS scattering patterns of the pure as cast **PT-biTh** and **PT-TT** films in Fig. 3, where the degree of order of **PT-TT** is greater than that of **PT-biTh**.

In our previous studies, we found that the presence of fullerenes challenges the ability of D′–A–D–A–D′-type small molecules to crystallize and thus drive phase separation,[70] leading to low fill-factors and poor charge extraction in as-cast blend films.[27,28,30] This frustration by $PC_{70}BM$ further exaggerates the differences between **PT-biTh** and **PT-TT** caused by rotamer and dipolar diversity seen in Fig. 4. The relative degree of order achieved in BHJ blends for **PT-biTh** and **PT-TT** can be compared using the CCLs of the same molecular features in

 

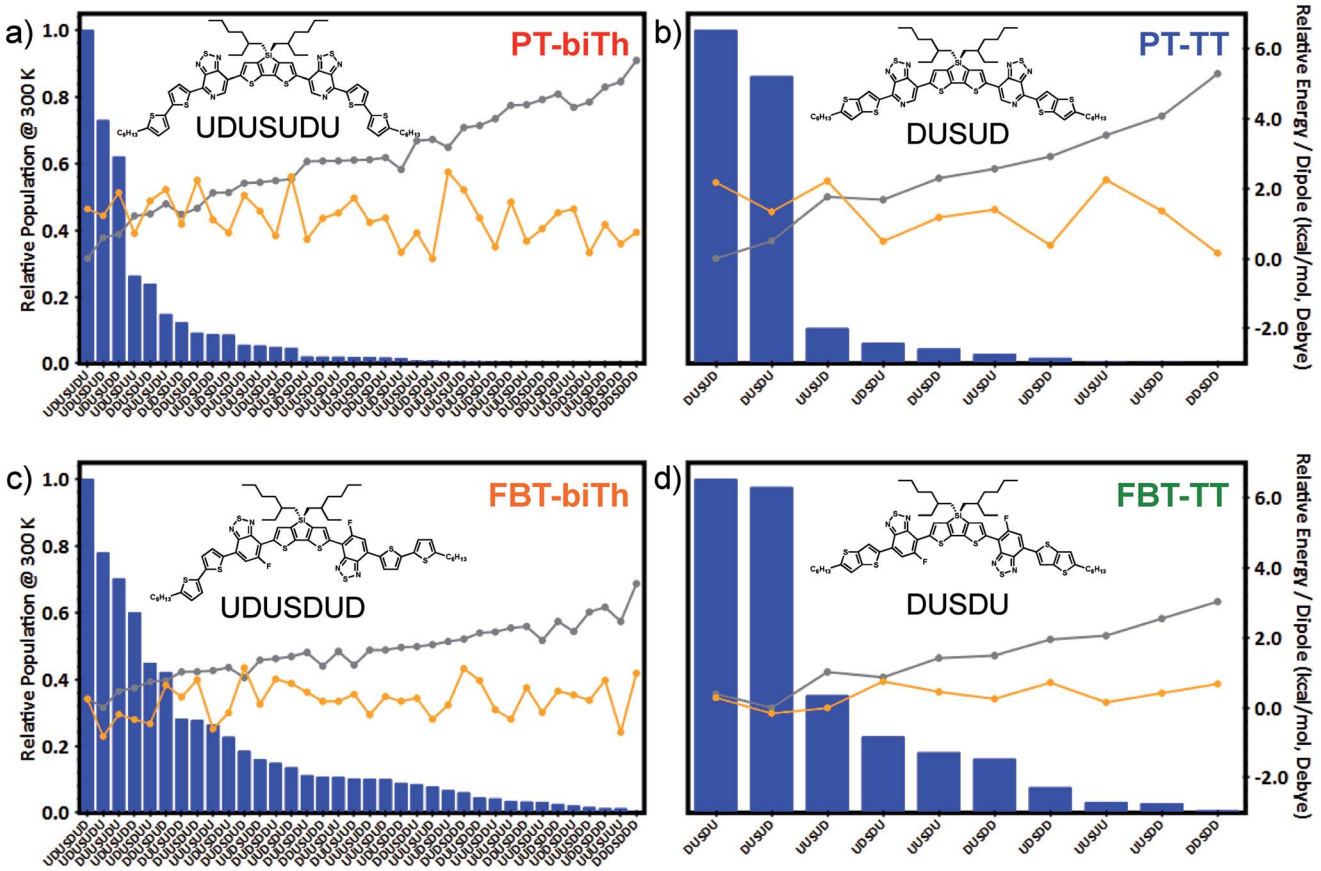


Fig. 10 The relative populations (blue), energies (grey) and short-axis dipole moment magnitudes (orange) for the unique planar rotamers described in Table S5† for (a) **PT-biTh**, (b) **PT-TT**, (c) **FBT-biTh**, and (d) **FBT-TT**. The relaxed potential energy (grey) is reported relative to the lowest energy rotamer. The structure of the rotamer with the largest probability and its designation are shown in the inset.

GIWAXS images in Fig. 7, presented in Table S1.† For example, the CCL of the alkyl-stacking peak of **PT-biTh** in as-cast blend films is significantly lower (at ~9 nm) than in neat films (35 nm). **PT-TT** exhibits a smaller drop in alkyl-stacking CCL from 32 nm to 13 nm and retains its higher-order diffraction spots, which suggests that it is less frustrated by fullerene by virtue of its narrower rotamer diversity. Thus, larger (or more perfect) donor crystallites form in **PT-TT**:$PC_{70}BM$ films which drives phase separation in as-cast blend films to achieve PCEs of 4.2% due to higher $J_{sc}$ and FF (47%). **PT-TT**'s more efficient charge extraction is indicative of a greater degree of phase separation than that of **PT-biTh**:$PC_{70}BM$ as-cast, having a PCE of 2.5% and a lower FF (37%).

Trends observed for **PT-biTh** and **PT-TT** extend to the FBT-containing molecules: the TT subunit reduces the rotamer population of **FBT-TT** to primarily four conformers, compared to ten for **FBT-biTh**. The reduced rotamer population is expected to facilitate assembly into ordered domains, which is confirmed by the increased definition of the diffraction features seen by GIWAXS in Fig. 4.[68] Furthermore, analysis of **FBT-biTh**'s and **FBT-TT**'s thermally-accessible rotamer populations may explain the reduced diffraction in both of their as-cast blend films in Fig. 8. Recall that the FBT-molecules have a more shallow energy landscape and thus more conformational dispersity than their PT-analogs. Indeed, the smaller energy differences give degeneracy more pronounced effects on their rotamer distribution, such that their most populated rotamer is the second lowest energy conformer and is asymmetric. This is expected to slow their relative rate of self-assembly (see Fig. S11 in the ESI† for a comparison of each molecules' two most populated rotamers). Additionally, rotamers of FBT-containing molecules exhibit less drastic shifts in dipole moment than their PT-analogs. The lowest energy conformers of **FBT-TT** have particularly low dipolar disorder compared to those of **FBT-biTh**, such that the different rotamer conformations could still be stabilized together in an ordered lattice.[28] Thus, **FBT-TT** may be able to more readily form interconnected donor domains than **FBT-biTh**.

Note that lowest energy rotamers of **PT-biTh** and **FBT-biTh** are in the same configuration, labeled UDUSUDU. This "banana" shape is observed for the single crystal structures of proximal **PT-biTh**.[71] The most populated **FBT-TT** rotamer is predicted to be DUSDU, which matches the primary conformation in the crystal structure in Fig. 5. Notably, this structure was resolved after theoretical analysis was completed. There are also partial contributions from less populous rotamers, such as DUSDD (ranked 6$^{th}$ most populous), DDSDU (8$^{th}$) and DDSDD (10$^{th}$). The reduced variation in dipole moment vectors between

the rotamers likely allows them to be readily accommodated into the same packing structure. Isolated single-crystals of **FBT-biTh** adopt a DUDSDUD (ranked 11$^{th}$) or DUDSDUU (14$^{th}$) conformation.[71] Unlike our original prediction that low energy states would be more influential in the crystal structure, this hints that certain molecular conformations are more favorable for forming stable solid-state lattices. These states may have a greater tendency to nucleate crystalline growth during film formation, regardless of their starting population. However, arguments on the resistance to crystallization due to a poorly compacted distribution of conformers and, particularly wide variation in dipole moment vectors, still apply under these conditions.

## Conclusions

We examined how a small change to molecular structure – substituting thienothiophene (TT) for bithiophene (biTh) – impacts the optical and electronic properties, self-assembly tendencies and ultimately photovoltaic performance of organic molecular semiconductors. Morphological studies show that this substitution leads to more distinct donor diffraction features in neat and bulk heterojunction blend films, indicating more facile self-assembly from solution.

We attribute the higher degree of self-assembly observed for **PT-TT** and **FBT-TT** to a reduction of conformational diversity relative to **PT-biTh** and **FBT-biTh**, respectively. Substituting the biTh subunit for TT reduces the number of points of rotation along the π-conjugated backbone. We calculated the relative energies and dipole moments of the possible conformations of each molecule in this tetrad, and found that TT-containing molecules have fewer thermally-accessible rotamers. Variations in the molecules' rotamer populations are consistent with the trends observed by GIWAXS, particularly the significantly increase in thin-film order for TT-containing molecules in blend films processed with DIO. We also found that FBT-containing molecules have higher degrees of thin-film order when compared to their PT counterparts. While substituting FBT for PT has complex influences on the material properties,[44,45] we can attribute changes in morphology, in part, to the smaller degree of dipolar disorder in the FBT molecules.

Increased rotamer dispersity exacerbates kinetic constraints during solution processing, such as competitive assembly of the acceptor $PC_{70}BM$ and varied drying time in bulk heterojunction films. Thus, the solar cell performance of the four molecular donors provides a practical demonstration of these effects. Both **PT-TT**:$PC_{70}BM$ and **FBT-TT**:$PC_{70}BM$ significantly improve upon the as-cast OPV performance of their biTh-analogs, **PT-biTh**:$PC_{70}BM$ and **FBT-biTh**:$PC_{70}BM$, by virtue of their more facile self-assembly. **FBT-biTh** and **FBT-TT** have a greater number of populated states than their PT-analogs, which appears to frustrate their ability to phase separate from $PC_{70}BM$ in blend films. However, the thermally-accessible rotamers of the FBT-containing molecules exhibit lower dipole variation. The low dipolar dispersity of **FBT-TT**, in particular, may account for its more ideal bulk heterojunction morphology as-cast, resulting in a PCE of 5.4% that further improves to 8.8% when processed with DIO.

Within a similar molecular semiconductor framework, TT limits rotamer distribution relative to biTh and thus aids self-assembly without significantly changing desirable optical and electronic properties. As such, the impact of molecular subunits on rotamer diversity should be considered future materials design. Indeed, reduced conformational dispersity and thus more reliable self-assembly may factor into the recent successes of extended rigid or fused backbone systems in the solution-processable OSC field, such as ITIC.[72–75] More robust understanding of conformational entropy – such as the diversity of rotamer conformation, energy, and dipole moment – will help us translate molecular structure into the desired degree of solid-state ordering.

## Conflicts of interest

There are no conflicts to declare.

## Acknowledgements

Research at UCSB was supported by the Office of Naval Research, ONR Awards No. N00014-14-1-0580, N00014-16-1-2520, and N00014-14-1-0101. C. M. thanks Dr Simon Teat, staff scientist of Beamline 11.3.1 at the ALS, for refining the FBT-TT crystal structure. GIWAXS measurements and single-crystal diffraction were carried out at Beamline 7.3.3 (ref. 76) and 11.3.1 of the Advanced Light Source, respectively, a DOE Office of Science User Facility under contract no. DE-AC02-05CH11231. KN, BY, and TG thank the UGC, New Delhi for providing research fellowships. SPS thanks financial support from Indo-US BASE (Bhaskara Advanced Solar Energy) Fellowship program, Grant No. IUSSTF BASE Fellowship 2015/F-4 and from Indo-UK APEX project (Phase-II). RD thanks the UGC for the Junior Research Fellowship. The work at the University of Kentucky was supported by the Department of the Navy, Office of Naval Research, ONR Award No. N00014-16-1-2985. Supercomputing resources on the Lipscomb High Performance Computing Cluster were provided by the University of Kentucky Information Technology Department and Center for Computational Sciences (CCS).

## References

1 J. Roncali, P. Leriche and P. Blanchard, *Adv. Mater.*, 2014, **26**, 3821–3838.
2 R. Po and J. Roncali, *J. Mater. Chem. C*, 2016, **4**, 3677–3685.
3 S. D. Collins, N. A. Ran, M. C. Heiber and T.-Q. Nguyen, *Adv. Energy Mater.*, 2017, 1602242.
4 Y. Huang, E. J. Kramer, A. J. Heeger and G. C. Bazan, *Chem. Rev.*, 2014, **114**, 7006–7043.
5 H. Kang, W. Lee, J. Oh, T. Kim, C. Lee and B. J. Kim, *Acc. Chem. Res.*, 2016, **49**, 2424–2434.
6 L. J. Richter, D. M. DeLongchamp and A. Amassian, *Chem. Rev.*, 2017, **117**, 6332–6366.
7 M. A. Baklar, F. Koch, A. Kumar, E. B. Domingo, M. Campoy-Quiles, K. Feldman, L. Yu, P. Wobkenberg, J. Ball, R. M. Wilson, I. McCulloch, T. Kreouzis, M. Heeney,

 

T. Anthopoulos, P. Smith and N. Stingelin, *Adv. Mater.*, 2010, **22**, 3942–3947.
8 S. Kwon, H. Kang, J.-H. Lee, J. Lee, S. Hong, H. Kim and K. Lee, *Adv. Energy Mater.*, 2016, 1601496.
9 D. M. DeLongchamp, R. J. Kline, D. A. Fischer, L. J. Richter and M. F. Toney, *Adv. Mater.*, 2011, **23**, 319–337.
10 H. Huang, L. Yang, A. Facchetti and T. J. Marks, *Chem. Rev.*, 2017, **117**, 10291–10318.
11 J. Mei and Z. Bao, *Chem. Mater.*, 2014, **26**, 604–615.
12 Z.-H. Guo, N. Ai, C. R. McBroom, T. Yuan, Y.-H. Lin, M. Roders, C. Zhu, A. L. Ayzner, J. Pei and L. Fang, *Polym. Chem.*, 2016, **7**, 648–655.
13 J. R. Tumbleston, L. Yang, W. You and H. Ade, *Polymer*, 2014, **55**, 4884–4889.
14 W. Zhang, Z. Mao, N. Zheng, J. Zou, L. Wang, C. Wei, J. Huang, D. Gao and G. Yu, *J. Mater. Chem. C*, 2016, **4**, 9266–9275.
15 C. Zhu, A. U. Mu, Y.-H. Lin, Z.-H. Guo, T. Yuan, S. E. Wheeler and L. Fang, *Org. Lett.*, 2016, **18**, 6332–6335.
16 A. Nangia, *Acc. Chem. Res.*, 2008, **41**, 595–604.
17 A. J. Cruz-Cabeza and J. Bernstein, *Chem. Rev.*, 2014, **114**, 2170–2191.
18 R. Hilfiker, F. Blatter and M. von Raumer, in *Polymorphism*, ed. R. Hilfiker, Wiley-VCH Verlag GmbH & Co. KGaA, 2006, pp. 1–19.
19 J. Lu and S. Rohani, *Curr. Med. Chem.*, 2009, **16**, 884–905.
20 P. Upadhyay, A. K. Dantuluri, L. Kumar and A. K. Bansal, *J. Pharm. Sci.*, 2012, **101**, 1843–1851.
21 D. P. Otto and M. M. De Villers, *Curr. Drug Discovery Technol.*, 2017, **14**, 72–105.
22 N. E. Jackson, B. M. Savoie, K. L. Kohlstedt, M. Olvera de la Cruz, G. C. Schatz, L. X. Chen and M. A. Ratner, *J. Am. Chem. Soc.*, 2013, **135**, 10475–10483.
23 N. E. Jackson, B. M. Savoie, K. L. Kohlstedt, T. J. Marks, L. X. Chen and M. A. Ratner, *Macromolecules*, 2014, **47**, 987–992.
24 N. E. Jackson, K. L. Kohlstedt, B. M. Savoie, M. Olvera de la Cruz, G. C. Schatz, L. X. Chen and M. A. Ratner, *J. Am. Chem. Soc.*, 2015, **137**, 6254–6262.
25 B. Kuei and E. D. Gomez, *Soft Matter*, 2016, **13**, 49–67.
26 J. E. Coughlin, Z. B. Henson, G. C. Welch and G. C. Bazan, *Acc. Chem. Res.*, 2014, **47**, 257–270.
27 Z. B. Henson, G. C. Welch, T. van der Poll and G. C. Bazan, *J. Am. Chem. Soc.*, 2012, **134**, 3766–3779.
28 C. J. Takacs, Y. Sun, G. C. Welch, L. A. Perez, X. Liu, W. Wen, G. C. Bazan and A. J. Heeger, *J. Am. Chem. Soc.*, 2012, **134**, 16597–16606.
29 T. S. van der Poll, A. Zhugayevych, E. Chertkov, R. C. Bakus, J. E. Coughlin, S. J. Teat, G. C. Bazan and S. Tretiak, *J. Phys. Chem. Lett.*, 2014, **5**, 2700–2704.
30 J. A. Love, C. M. Proctor, J. Liu, C. J. Takacs, A. Sharenko, T. S. van der Poll, A. J. Heeger, G. C. Bazan and T.-Q. Nguyen, *Adv. Funct. Mater.*, 2013, **23**, 5019–5026.
31 L. A. Perez, K. W. Chou, J. A. Love, T. S. van der Poll, D.-M. Smilgies, T.-Q. Nguyen, E. J. Kramer, A. Amassian and G. C. Bazan, *Adv. Mater.*, 2013, **25**, 6380–6384.
32 Q. Zhao, X. Yu, J. Liu, Z. Xie and Y. Han, *Org. Electron.*, 2016, **37**, 6–13.
33 M. Reichenberger, J. A. Love, A. Rudnick, S. Bagnich, F. Panzer, A. Stradomska, G. C. Bazan, T.-Q. Nguyen and A. Köhler, *J. Chem. Phys.*, 2016, **144**, 74904.
34 G.-Y. Chen, Y.-H. Cheng, Y.-J. Chou, M.-S. Su, C.-M. Chen and K.-H. Wei, *Chem. Commun.*, 2011, **47**, 5064–5066.
35 J. S. Lee, S. K. Son, S. Song, H. Kim, D. R. Lee, K. Kim, M. J. Ko, D. H. Choi, B. Kim and J. H. Cho, *Chem. Mater.*, 2012, **24**, 1316–1323.
36 C. woo Jeon, S.-H. Kang, H.-J. Yun, T. K. An, H. Cha, C.-E. Park and Y.-H. Kim, *Synth. Met.*, 2013, **185–186**, 159–166.
37 A. J. Pearson, D. C. Watters, H. Yi, M. S. Sarjadi, L. X. Reynolds, P. P. Marchisio, J. Kingsley, S. A. Haque, A. Iraqi and D. G. Lidzey, *RSC Adv.*, 2014, **4**, 43142–43149.
38 C. K. Lo and J. R. Reynolds, *Polymer*, 2016, **99**, 741–747.
39 M. Abdelsamie, K. Zhao, M. R. Niazi, K. W. Chou and A. Amassian, *J. Mater. Chem. C*, 2014, **2**, 3373–3381.
40 J. Mei, K. R. Graham, R. Stalder and J. R. Reynolds, *Org. Lett.*, 2010, **12**, 660–663.
41 S. W. Yun, J. H. Kim, S. Shin, H. Yang, B.-K. An, L. Yang and S. Y. Park, *Adv. Mater.*, 2012, **24**, 911–915.
42 Y. An, D. X. Long, Y. Kim, Y.-Y. Noh and C. Yang, *Phys. Chem. Chem. Phys.*, 2016, **18**, 12486–12493.
43 R. Noriega, J. Rivnay, K. Vandewal, F. P. V. Koch, N. Stingelin, P. Smith, M. F. Toney and A. Salleo, *Nat. Mater.*, 2013, **12**, 1038–1044.
44 J. Yuan, N. A. Ran, M. J. Ford, M. Wang, M. Kumar Ravva, C.-K. Mai, X. Liu, J.-L. Brédas, T.-Q. Nguyen, W. Ma and G. C. Bazan, *J. Mater. Chem. A*, 2017, **5**, 18618–18626.
45 J. H. Yun, S. Park, J. H. Heo, H.-S. Lee, S. Yoon, J. Kang, S. H. Im, H. Kim, W. Lee, B. Kim, M. J. Ko, D. S. Chung and H. J. Son, *Chem. Sci.*, 2016, **7**, 6649–6661.
46 D.-M. Smilgies and D. R. Blasini, *J. Appl. Crystallogr.*, 2007, **40**, 716–718.
47 M. Abdelsamie, N. D. Treat, K. Zhao, C. McDowell, M. A. Burgers, R. Li, D.-M. Smilgies, N. Stingelin, G. C. Bazan and A. Amassian, *Adv. Mater.*, 2015, **27**, 7285–7292.
48 K. Vakhshouri, B. H. Smith, E. P. Chan, C. Wang, A. Salleo, C. Wang, A. Hexemer and E. D. Gomez, *Macromolecules*, 2016, **49**, 7359–7369.
49 X. Chen, X. Liu, M. A. Burgers, Y. Huang and G. C. Bazan, *Angew. Chem., Int. Ed.*, 2014, **53**, 14378–14381.
50 C. Sprau, F. Buss, M. Wagner, D. Landerer, M. Koppitz, A. Schulz, D. Bahro, W. Schabel, P. Scharfer and A. Colsmann, *Energy Environ. Sci.*, 2015, **8**, 2744–2752.
51 T. S. van der Poll, J. A. Love, T.-Q. Nguyen and G. C. Bazan, *Adv. Mater.*, 2012, **24**, 3646–3649.
52 A. K. K. Kyaw, D. H. Wang, C. Luo, Y. Cao, T.-Q. Nguyen, G. C. Bazan and A. J. Heeger, *Adv. Energy Mater.*, 2014, **4**, 1301469.
53 D. H. Wang, P.-O. Morin, C.-L. Lee, A. K. K. Kyaw, M. Leclerc and A. J. Heeger, *J. Mater. Chem. A*, 2014, **2**, 15052–15057.
54 A. Zusan, B. Gieseking, M. Zerson, V. Dyakonov, R. Magerle and C. Deibel, *Sci. Rep.*, 2015, **5**, 8286.

55 Y. Sun, G. C. Welch, W. L. Leong, C. J. Takacs, G. C. Bazan and A. J. Heeger, *Nat. Mater.*, 2012, **11**, 44–48.
56 Y. Zhang, X.-D. Dang, C. Kim and T.-Q. Nguyen, *Adv. Energy Mater.*, 2011, **1**, 610–617.
57 D. Bartesaghi, I. d. C. Pérez, J. Kniepert, S. Roland, M. Turbiez, D. Neher and L. J. A. Koster, *Nat. Commun.*, 2015, **6**, 7083.
58 M.-H. Jao, H.-C. Liao and W.-F. Su, *J. Mater. Chem. A*, 2016, **4**, 5784–5801.
59 B. Kan, Q. Zhang, M. Li, X. Wan, W. Ni, G. Long, Y. Wang, X. Yang, H. Feng and Y. Chen, *J. Am. Chem. Soc.*, 2014, **136**, 15529–15532.
60 Q. Zhang, B. Kan, F. Liu, G. Long, X. Wan, X. Chen, Y. Zuo, W. Ni, H. Zhang, M. Li, Z. Hu, F. Huang, Y. Cao, Z. Liang, M. Zhang, T. P. Russell and Y. Chen, *Nat. Photonics*, 2015, **9**, 35–41.
61 V. Gupta, L. F. Lai, R. Datt, S. Chand, A. J. Heeger, G. C. Bazan and S. P. Singh, *Chem. Commun.*, 2016, **52**, 8596–8599.
62 P. Müller-Buschbaum, *Adv. Mater.*, 2014, **26**, 7692–7709.
63 C. McDowell, M. Abdelsamie, K. Zhao, D.-M. Smilgies, G. C. Bazan and A. Amassian, *Adv. Energy Mater.*, 2015, **5**, 1501121.
64 J. E. Coughlin, A. Zhugayevych, R. C. Bakus, T. S. van der Poll, G. C. Welch, S. J. Teat, G. C. Bazan and S. Tretiak, *J. Phys. Chem. C*, 2014, **118**, 15610–15623.
65 W. Zhang, K. Shi, J. Huang, D. Gao, Z. Mao, D. Li and G. Yu, *Macromolecules*, 2016, **49**, 2582–2591.
66 G. Raos, A. Famulari and V. Marcon, *Chem. Phys. Lett.*, 2003, **379**, 364–372.
67 S. B. Darling and M. Sternberg, *J. Phys. Chem. B*, 2009, **113**, 6215–6218.
68 J. Rivnay, R. Noriega, R. J. Kline, A. Salleo and M. F. Toney, *Phys. Rev. B: Condens. Matter Mater. Phys.*, 2011, **84**, 45203.
69 I. N. Levine, *Physical chemistry*, McGraw-Hill, 2008.
70 A. Sharenko, M. Kuik, M. F. Toney and T.-Q. Nguyen, *Adv. Funct. Mater.*, 2014, **24**, 3543–3550.
71 G. C. Welch, R. C. Bakus, S. J. Teat and G. C. Bazan, *J. Am. Chem. Soc.*, 2013, **135**, 2298–2305.
72 Y. Lin, J. Wang, Z.-G. Zhang, H. Bai, Y. Li, D. Zhu and X. Zhan, *Adv. Mater.*, 2015, **27**, 1170–1174.
73 Y. Lin, F. Zhao, Q. He, L. Huo, Y. Wu, T. C. Parker, W. Ma, Y. Sun, C. Wang, D. Zhu, A. J. Heeger, S. R. Marder and X. Zhan, *J. Am. Chem. Soc.*, 2016, **138**, 4955–4961.
74 N. Qiu, H. Zhang, X. Wan, C. Li, X. Ke, H. Feng, B. Kan, H. Zhang, Q. Zhang, Y. Lu and Y. Chen, *Adv. Mater.*, 2017, **29**, 1604964.
75 B. Zhao, C. Yan, Z. Wang, H. Huang, Y. Hu, P. Cheng, M. Yi, C. Huang, X. Zhan and W. Huang, *J. Mater. Chem. C*, 2017, **5**, 8988–8998.
76 A. Hexemer, W. Bras, J. Glossinger, E. Schaible, E. Gann, R. Kirian, A. MacDowell, M. Church, B. Rude and H. Padmore, *J. Phys.: Conf. Ser.*, 2010, **247**, 12007.

 